NATIONAL AERONAUTICS AND SPACE ADMINISTRATION

Technical Report 32-1352

Large Spacecraft Antenna Study Analytical Pattern Subtask

R. M. Dickinson

JET PROPULSION LABORATORY
CALIFORNIA INSTITUTE OF TECHNOLOGY
PASADENA, CALIFORNIA

January 15, 1969

TECHNICAL REPORT 32-1352

Prepared Under Contract No. NAS 7-100
National Aeronautics and Space Administration

Preface

The work described in this report was performed by the Telecommunications Division of the Jet Propulsion Laboratory.

Contents

I. Introduction 1

II. Analysis 1
A. Surfaces 1
B. Coordinate System 2
C. Polarization 3
D. Integrating Surface Current 3
E. Focus Location for Greatest Gain 4

III. Experiment 4
A. Reflector 4
B. Feeds 4

IV. Results 7
A. Patterns 7
B. Aperture Efficiency 8
C. Erectable Surface Loss 9

V. Conclusions and Recommendations 11

Appendix A. Equations 12

Appendix B. Computer Programs 18

References 26

Table

1. Primary illuminator characteristics at 2297.6 MHz 6

Figures

1. Coordinate system 2
2. Six-rib model erectable reflector 5
3. Eight-rib model erectable reflector 6
4. Circular cupped turnstile performance 7
5. Hybrid-fed feed performance 8
6. Phase errors vs focal position for hybrid-fed feed in 6-rib dish 8
7. Measured and calculated 6-rib dish patterns 9
8. Measured and calculated 8-rib dish patterns 10
9. Illuminator aperture efficiency in a perfect paraboloid 10
A-1. Gore panel layout pattern 12
A-2. Gore geometry of a gored surface 13
A-3. The straight-rib geometry 15
A-4. The circular-rib geometry 15

Abstract

This report presents the results of an analytic and experimental program to develop techniques for calculating the circularly polarized patterns of erectable spacecraft high-gain antennas. Surface equations for one class of radial rib erectable antenna are derived. Mathematical expressions are developed for calculating the far field circularly polarized patterns based upon the reflector surface equations and circularly polarized feed illumination patterns.

Experimental measured patterns were obtained to compare with the computer calculated theoretical patterns. Sample computer programs used to obtain the best focus position and to calculate patterns are contained in the Appendix.

Large Spacecraft Antenna Study
Analytical Pattern Subtask

I. Introduction

The objective of this subtask was to develop an analytic method for calculating the patterns of high-gain unfurlable spacecraft antennas. Because of the mechanical compromises necessary for packaging the antennas, the erected surfaces are not smooth paraboloids, but only an approximation.

The subtask consisted of three parts:

(1) Part one consisted of deriving the surface equations of one type of erectable surface: the radial rib antenna.

(2) Part two was the analytical development of mathematical expressions for calculating the far field patterns of erectable spacecraft antennas. Most of the equations developed during this study will be relegated to the appendix.

(3) Part three was an experimental program to obtain measured patterns of erectable antenna models for comparison with the calculated patterns.

II. Analysis

The technique selected for calculating patterns uses surface current integration as outlined in Section 5.9 of Ref. 1. Significant features of the particular implementation of this technique are:

(1) A unified coordinate system is used to describe the primary pattern, the reflector surface, and the secondary pattern.

(2) A system of circularly polarized unit vectors is employed to handle the primary and secondary pattern polarization.

(3) Only the surface position vector equation need be derived. The surface unit normal and element of area are contained within the particular formulation.

A. Surfaces

The reflecting surfaces are described in equation form by giving the magnitude of a position vector directed from the coordinate origin to the surface for each value of the position vector direction angles. For example, with reference to Fig. 1, the vector surface equation is

$$\boldsymbol{\rho} = \rho(\theta, \phi)\,\mathbf{i}_\rho \tag{1}$$

where θ, ϕ are the spherical coordinate angles and $\mathbf{i}_\rho$ is the unit vector in the direction of increasing ρ.

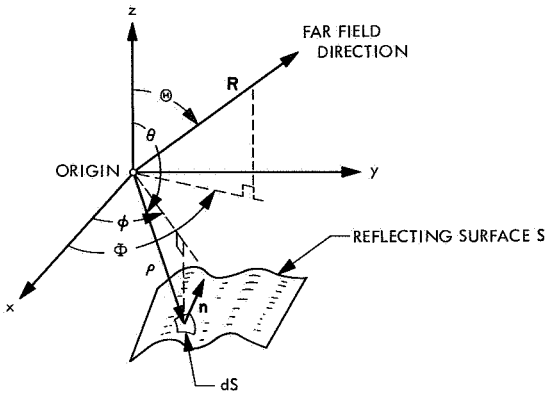

Fig. 1. Coordinate system

The true erectable antenna surface in the space environment can only be derived from mainly mechanical considerations. These considerations involve balancing the forces acting upon the reflecting surface. The forces that shape the reflecting material arise from the following inputs:

(1) Stress properties of the reflecting material.

(2) Thermal properties.

(3) The antenna erecting mechanism.

(4) Spacecraft attitude control forces.

(5) Solar electromagnetic forces.

(6) Spacecraft electrostatic or magnetostatic forces.

Since surface equations were not available for the above conditions, a derivation was made of a particular theoretical model of one class of erectable surface—the radial rib antenna.

The radial rib antenna consists of reflecting material pulled uniformly between pairs of radial ribs. In the theoretical model the material has no sag or deviation from a straight line between equidistant radial points along a rib pair: the resulting surface is termed a *gore*, a term used in dressmaking.

If normal fabric type reflecting material is used for the antenna, the gore will support two-dimensional curvature to balance the forces caused by the ribs and the resulting unequal orthogonal tensions in the fabric. The billowing or double curvature of the fabric surface is termed *the upholstery effect*. In the following discussion, the reflecting material will be assumed to support a singly-curved surface only.

The derivation of the equations for a general singly-curved, gored surface with radial ribs (Ref. 2) is outlined in Appendix A.

The surface current integration technique as formulated in Ref. 1 requires the equations of not only the surface, but also the surface unit normal **n**, and the elemental surface area dS.

As the surface equations alone are difficult to obtain, these additional requirements should be obtained as simply as possible.

By using differential geometry (Refs. 3 and 4), the surface unit normal is

$$\mathbf{n} = \frac{\dfrac{\partial \boldsymbol{\rho}}{\partial \phi} \times \dfrac{\partial \boldsymbol{\rho}}{\partial \theta}}{(EG - F^2)^{1/2}} \tag{2}$$

and the element of area is given by

$$dS = (EG - F^2)^{1/2}\, d\theta\, d\phi \tag{3}$$

where

$$E = \frac{\partial \boldsymbol{\rho}}{\partial \theta} \cdot \frac{\partial \boldsymbol{\rho}}{\partial \theta}, \qquad F = \frac{\partial \boldsymbol{\rho}}{\partial \phi} \cdot \frac{\partial \boldsymbol{\rho}}{\partial \theta}, \qquad G = \frac{\partial \boldsymbol{\rho}}{\partial \phi} \cdot \frac{\partial \boldsymbol{\rho}}{\partial \phi} \tag{4}$$

The common radical term will cancel leaving only vector partial derivatives in the surface current formulation.

B. Coordinate System

To simplify the derivation of the surface current integrand, it was decided to specify the coordinate origin to be the primary illuminator phase center. Other choices could have been the reflector vertex, or the intersection of the focal axis with the aperture plane, etc. Also, a spherical polar coordinate system is used.

These choices complicate the derivation of the surface equation but sidestep the many transformations required if feed, reflector, and secondary pattern are separately described relative to their own coordinate system. Also, the feed pattern corresponds to the output of normal pattern measurement practice with respect to the Z-axis, but with the $\theta = 0$ and $\theta = \pi$ directions simply reversed as shown in Fig. 1.

The secondary pattern is the vector sum of the feed direct radiation and the scattered radiation from the reflector. This addition is simplified by calculating the scattered radiation relative to the feed phase center.

Calculating the secondary pattern with respect to the feed phase center should not cause any difficulty except perhaps if the secondary pattern is to be used as the primary illuminator for another larger reflector. In which case it would be desirable to calculate the secondary pattern phase relative to its own phase center.

C. Polarization

Since most spacecraft antennae are designed to radiate circularly polarized radiation, it is desirable to perform pattern calculations using circularly polarized field components (Ref. 5).

A system of unit vectors with restrictions (Refs. 6 and 7) has been contrived to represent circularly polarized radiation in portions of the spherical coordinate system. The unit vector defining the polarization of the feed field directed toward the reflector is given for left hand circularly polarized radiation as

$$\mu_L = 2^{-1/2}(\mathbf{i}_\theta + j\,\mathbf{i}_\phi)\exp -j\phi \qquad \text{for } 0 < \theta \leq \pi, \text{any } \phi \tag{5}$$

The unit vectors $\mathbf{i}_\theta$ and $\mathbf{i}_\phi$ are by definition normal to the direction of propagation, $\mathbf{i}_\rho$. However, at the poles of the coordinate system, their direction is ambiguous. With respect to the cartesian coordinate system of Fig. 1 in which the spherical coordinate system is immersed, the polarization vectors are defined to be oriented parallel to the X- and Y-axes at one pole (generally the peak of the pattern) and left undefined at the opposite pole (generally the pattern null opposite the peak). The exp $-j\phi$ term fixes the orientation of the two spatially orthogonal, time quadrature vectors in the coordinate system. This is required because $\mathbf{i}_\theta$ and $\mathbf{i}_\phi$ change direction with ϕ. The far field unit polarization vector is normal to the direction of propagation and is given for right circular polarization by

$$\mu'_R = 2^{-1/2}(\mathbf{i}_\Theta + j\,\mathbf{i}_\Phi)\exp j\Phi \qquad \text{for } 0 \leq \Theta < \pi, \text{any } \Phi \tag{6}$$

However, to perform the dot product of the complex conjugate of this vector with the surface current in order to obtain the far field components, it is necessary to obtain Eq. (6) in terms of $\mathbf{i}_\rho, \mathbf{i}_\theta, \mathbf{i}_\phi$. This relation (Ref. 8) is given in Appendix A.

Equations (11) and (12) in Ref. 8 give the final mathematical expressions for calculating circularly polarized far field patterns incorporating the features described above.

D. Integrating Surface Current

The calculation of far field patterns requires the evaluation of a double integral (Eq. 11, Ref. 8) over the erectable antenna surface. The integration must be performed numerically on a computer due to its complexity (Ref. 9).

The first programming attempts used a double Simpson (Ref. 10) integration scheme wherein the integrand was calculated over each gore of the reflector at points evenly spaced in the spherical coordinate variables. The evenly spaced coordinate points allowed the use of simple finite difference techniques for evaluating the surface derivatives. However, the spherical coordinates cause a grouping of points near the pole or vertex of the reflector and widespread points near the reflector edge.

Since approximately 5 points per wavelength on the surface are required for good accuracy, the first scheme leads to an inordinate number of points to be evaluated around the pole at $\theta = \pi$.

The second programming attempt took advantage of the fact that since each gore is identical, the surface vector magnitude and its derivatives need only be calculated for one gore. Appropriate angular changes are made in the calculations to reflect the different gore positions around the focal axis. In addition, the surface arc length for a paraboloid is used to calculate an approximately equal area distribution of points over the surface at which the integrand is to be evaluated. The latter scheme requires less computer time, but analytic surface derivatives are needed. The program is shown in Appendix B.

The integration is still performed by a Simpson method but uses single integration in one variable, the results of which are then singly integrated again in the other variable.[1]

[1]It was noted in a private communication with Mr. Arthur Ludwig that he has developed an integration scheme which requires only about 1½ points per wavelength on the surface for the same accuracy as a Simpson scheme. However, the Ludwig method has not as yet been incorporated into the above program.

An attempt was made to develop a general program input to handle a wide range of reflecting surfaces (e.g., spacecraft solar panels), but the possible range of reflector surface geometries and their boundaries greatly complicate any simple schemes for the method of selecting surface current integration points. Nonetheless, the mathematical development is still applicable, requiring only the particular reflecting surface equation and illuminator characteristics. For each particular type reflector the computer program must be restructured to calculate a grid of surface current integration points that lie only within the reflector boundaries.

E. Focus Location for Greatest Gain

Since an erectable antenna reflector surface only approximates a paraboloid, the feed location for greatest gain cannot be readily located by reference to the surface geometry. However, for a given feed pattern, the best focus position can be determined from the criteria (Ref. 11) that the illumination weighted mean phase deviation over the aperture be zero.

A computer program was written which uses a random number generator to provide coordinates for sampling the phase deviation over the reflector surface for a given focus position. Each sample point is weighted by the feed pattern and the sum of all sample points is averaged to yield the weighted average phase deviation. The best focus location is determined from a plot of mean phase deviation vs focus position. The program is shown in Appendix A.

III. Experiment

A. Reflector

Two models of radial parabolic rib erectable antennas were constructed to be used for checking the accuracy of the pattern and best focus location calculating programs.

Figure 2 shows the 3-ft diam 6-rib model, and Fig. 3 the 6-ft diam 8-rib model. The 0.35 focal length to diameter ratio (F/D) ribs were made from saw cut stacks of aluminum sheet. The parabolic template curve was obtained from a computer generated and plotted curve.

The gore reflecting material is 2,000 Å aluminized 1-mil mylar, attached to the ribs by film splicing tape. A pattern for use in cutting the gores was also generated and plotted by computer.

B. Feeds

Two types of circularly-polarized feeds were constructed for illuminating the model erectable surfaces at the frequency of 2297.6 MHz.

One feed is a column-supported, crossed turnstile fed with a half-wavelength split-balun. The feed has a circular cup reflector. The second feed which was tripod-supported in the 3-ft dish consists of a hybrid-fed coaxial slot backed up with a cup which provides uniform ellipticity over the pattern and a 5.5-in. diam ground plane for back-lobe suppression.

Problems were encountered with both the phase centers and polarization characteristics of the feeds. The cupped turnstile feed dipole elements were adjusted for minimum (0.3 dB) ellipticity on axis for the feed alone. The feed was then placed in the 3-ft diam model reflector and positioned for greatest secondary pattern gain with respect to a right circularly-polarized illuminator (0.25-dB ellipticity). The on-axis ellipticity of the secondary pattern was 4.5 dB! Ideally, the secondary pattern ellipticity should reflect the primary pattern ellipticity.

The feed was then adjusted for greatest gain and minimum ellipticity simultaneously while installed in the 6-rib model reflector. The secondary pattern ellipticity was then 0.3 dB. However, the ellipticity of the feed alone was determined to be 4.0 dB. Figure 4a shows the circular cupped turnstile feed performance as the feed is moved axially in the dish. A possible explanation for the polarization difficulty is that the portion of the reflected radiation from the dish that is intercepted by the feed is again reradiated by the feed in the same sense (thus cross-polarized with respect to the feed). Upon scattering from the dish a second time, the feed-intercepted reradiation is of opposite sense to the main beam dominant polarization.

Next, the phase center of the feed alone was measured and was determined to be 0.19 in. in front of the cup lip. The location of the cup lip from the vertex for greatest gain was 10.27 in. which made the best focal length equal to 10.08 in. It was thought that the feed phase center should be located at the mean geometrical focus of the reflector. The ribs are parabolic with a focal length of 12.6 in. The gores are wedges of parabolic cylinders with a focal length of 9.4 in. The mean focus is thus 11.0 in.

At the same time these measurements were being made, the first results were available from the pattern calculating program. The calculated patterns were wider than the

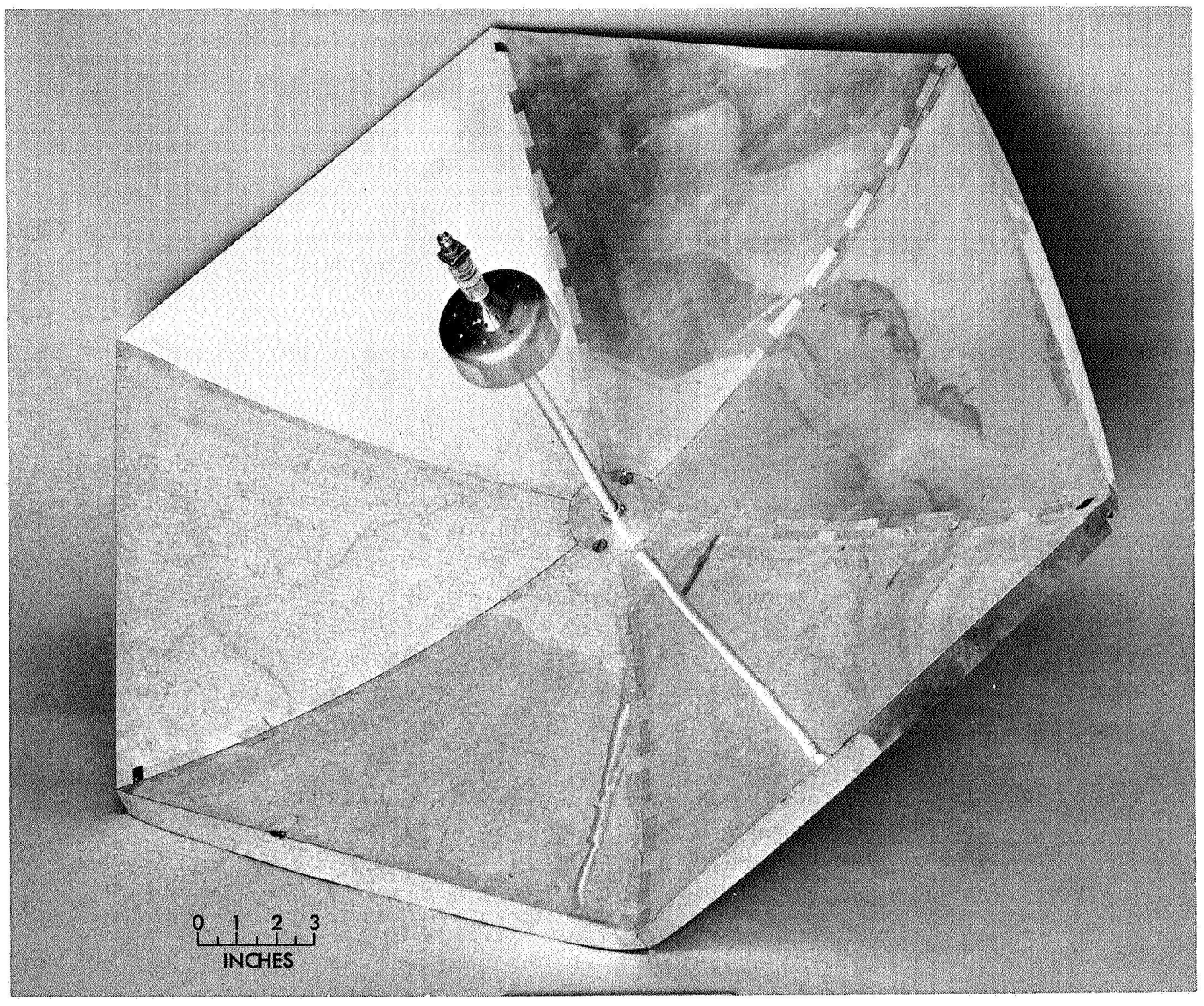

Fig. 2. Six-rib model erectable reflector

measured patterns although the peak gain approximately agreed.

It was decided to construct the quadrature hybrid-fed feed on the theory that its ellipticity and phase center location would be less sensitive to reaction from the reflector;[2] this was based on: (1) the changed feed ellipticity in the reflector, (2) the difference in focal position, and (3) the wider calculated patterns. The gain calculating program requires as input the primary illuminator gain pattern and phase center while in the reflector. Those data are presently obtained by measurements on the feed alone. The assumption is made that the feed characteristics do not change when the feed is mounted in the reflector.

The two illuminator characteristics are given in Table 1. The feed amplitude patterns are rotationally symmetric within ± 0.5 dB and the phase patterns are constant within ± 6 deg over the portion of the main beam that illuminates the reflector. The ellipticity increases approximately linearly off axis to less than 2 dB over the same angular region. The hybrid fed feed has a narrower beamwidth and thus should have greater gain than the cupped

[2]The hybrid would assure equal power division in two orthogonal components with the desired quadrature phase relation for circular polarization.

Table 1. Primary illuminator characteristics at 2297.6 MHz

Feed	Diam, in.	−3-dB beamwidth, deg	−10-dB beamwidth, deg	Peak gain, dB	Cross-polarized backlobe level, dB	Cross-polarized on axis, dB	Main beam representation in dB as a function of angle in radians, $\pi/2 < \theta \leq \pi$
Cupped turnstile	3.5	77	159	7.6	−15.5	−24	$G = 3.418\,\theta^2 + 23.98\,\theta - 33.88$
Hybrid fed	5.5	73	144	7.5	−22.0	−30	$G = -1.419\,\theta^3 + 5.183\,\theta^2 + 9.485\,\theta - 29.482$

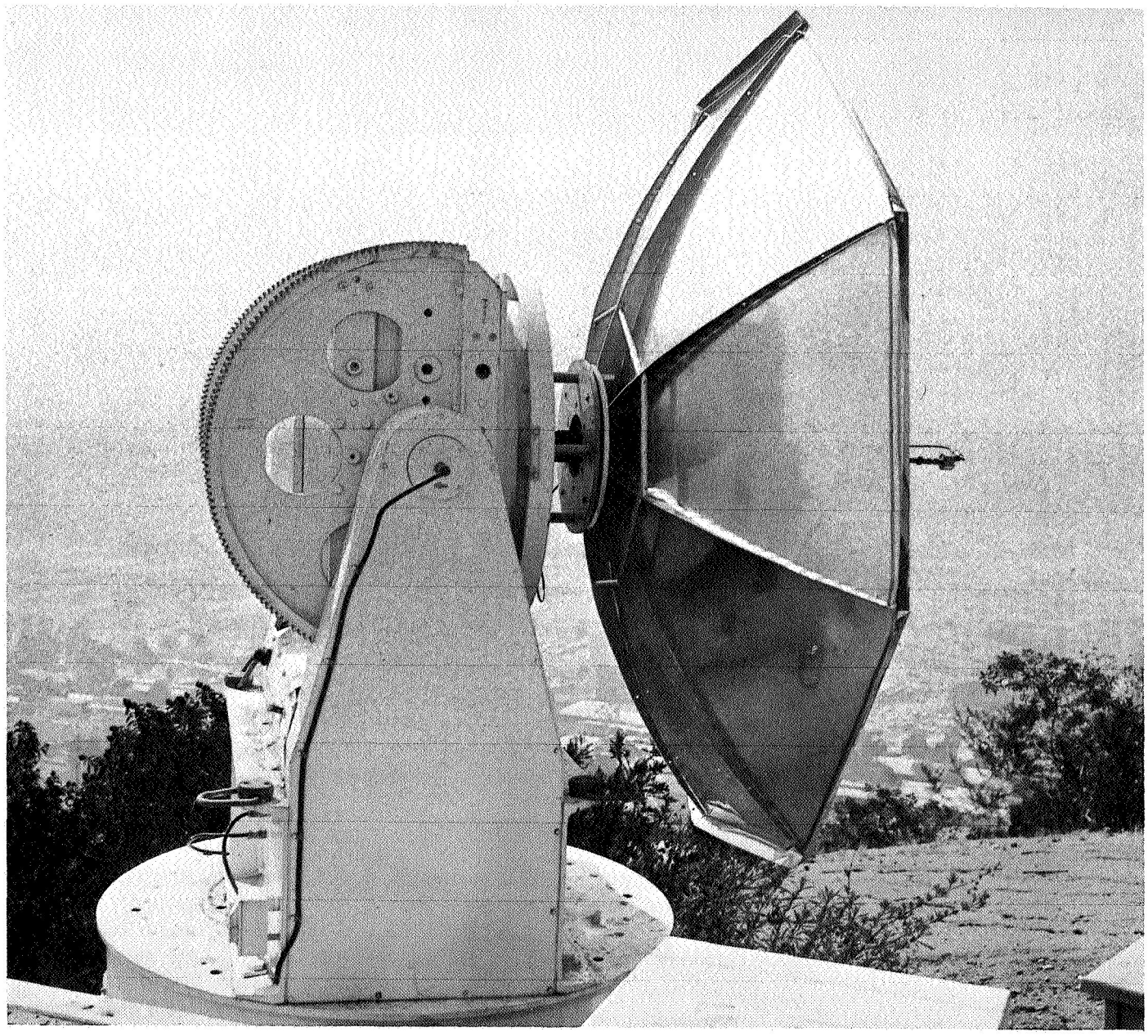

Fig. 3. Eight-rib model erectable reflector

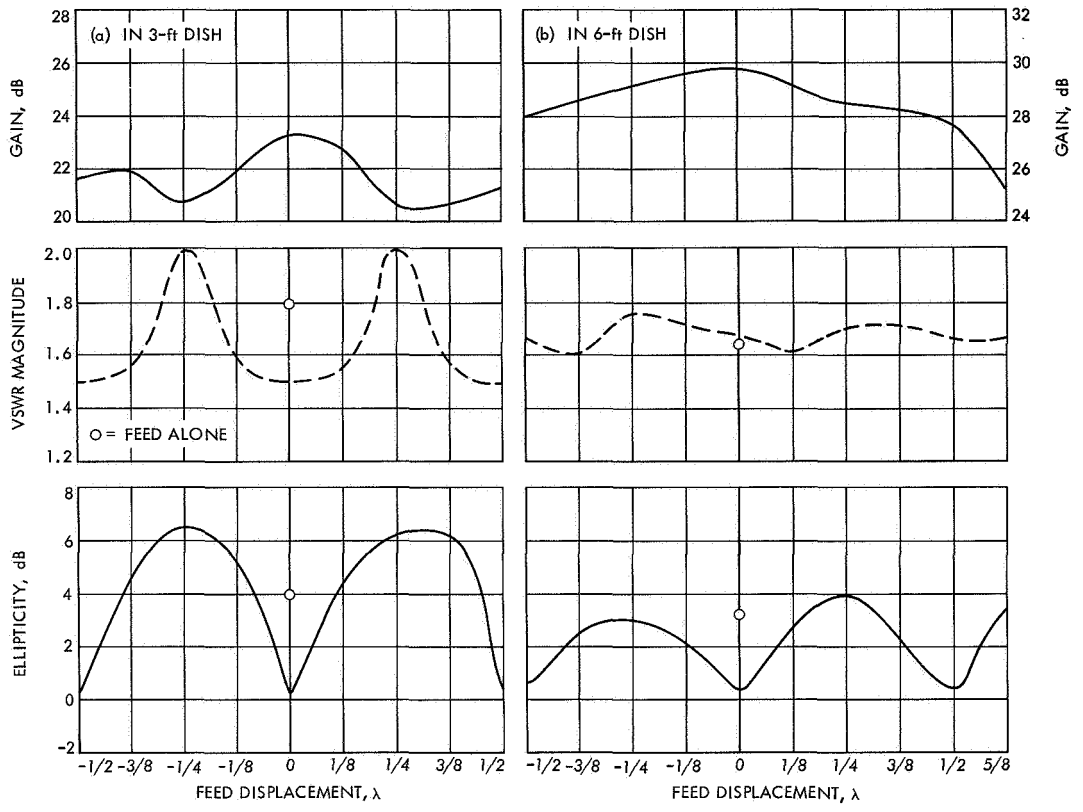

Fig. 4. Circular cupped turnstile performance

turnstile feed. However, the hybrid losses reduce the available gain.

The measured performance of the hybrid fed feed is shown in Fig. 5. The ellipticity and VSWR are approximately the same in or out of the dish. The changing reflected power with focal length, which is cross polarized, appears in the terminated port of the hybrid, whereas Fig. 4a shows that the cupped turnstile VSWR and ellipticity are most seriously affected by focal position.

The phase center of the hybrid fed feed was measured to be 0.12 in. behind the mouth of the coaxial cavity. The focal length for greatest gain in the 6-rib dish was not 11 in. but measured 10.36 in.

The discrepancy between the assumed and measured best focus was resolved by the illumination weighted mean phase technique discussed in Section II-E. Figure 6 shows a plot of the illumination weighted mean phase error and mean square phase error as a function of focal position for the hybrid-fed feed. The calculated best focus was 10.47 in., which agrees with the measured 10.36 in. within experimental error.

However, for the cupped turnstile, the similar calculated best focus location is 10.44 in. vs the measured 10.08 in. due to reflector reaction on the feed.

In order to overcome the effects of the reflector reaction modifying the feed characteristics in the short (2λ) focal length dish, the 6-ft diam 8-rib reflector model was constructed. The focal length is about 4λ for this model.

IV. Results

A. Patterns

Due to reflector reaction on the feed in the short focus 6-rib dish, the calculated patterns of the hybrid fed feed are still wider than the measured patterns as shown in Fig. 7. However, the agreement between measured (22.87 dB) and calculated (23.21 dB) peak gain is satisfactory, especially since the calculated gain is based upon a measurement of the low-gain feed peak gain (7.5 dB relative to circular isotropic). The gains are plotted on an absolute scale in Fig. 7. The calculated pattern does not account for any blockage by the hybrid fed feed or the ¼-in. diam rod, tripod feed support structure. Normally,

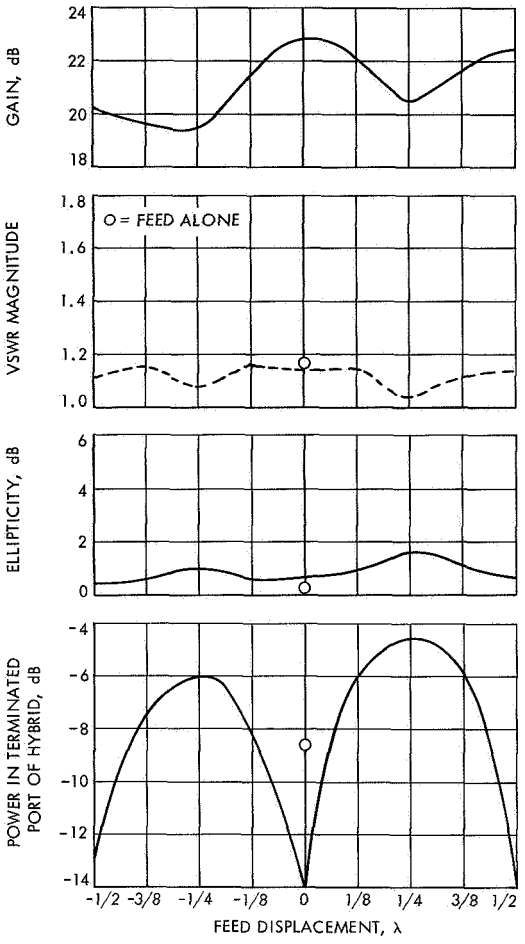

Fig. 5. Hybrid-fed feed performance

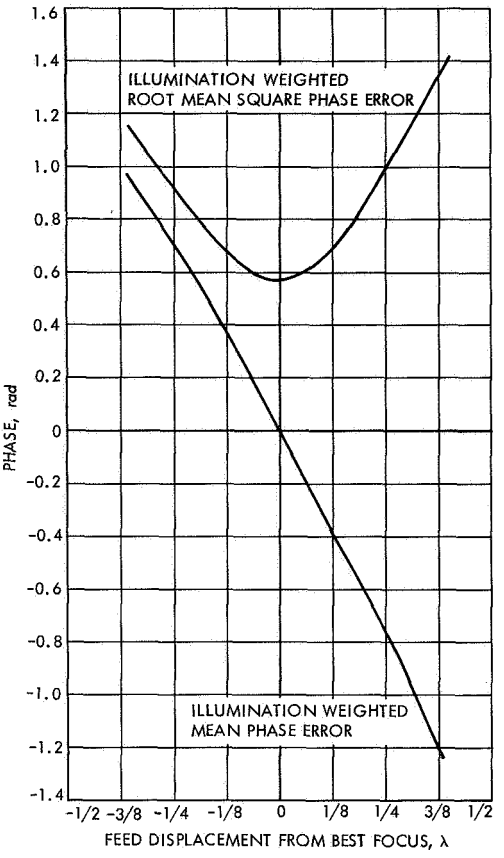

Fig. 6. Phase errors vs focal position for hybrid-fed feed in 6-rib dish

by not taking blockage into consideration, the calculated patterns should be narrower than the measured patterns.

For the longer focal length reflector, however, the agreement between measured and calculated pattern shape, peak gain and best focus position is greatly improved due to the lessened feed characteristic changes as shown in Fig. 4b.

Figure 8 shows the comparison between measured and calculated patterns of the 6-ft diam 8-rib dish with the column-supported circular cupped turnstile feed. The measured peak gain is 29.79 dB and the computer calculated peak gain is 30.00 dB. The measured best focus position is 22.75 in. and the computer calculated best focus position is 22.70 in.

The actual side lobe structure is expected to be different from the theoretical calculations, due to scattering from the feed and its support structure. Also, the pattern shape discrepancies are expected to be less for erectable antennas that better model a paraboloid. The surface current theory upon which the calculations are based contains the assumption that the reflecting surface does not have radii of curvature small compared to a wavelength. The interstices at the gore intersections represent serious departures from a smooth continuous surface.[3] Thus, the small reflector models provide an unrealistically severe test of the pattern calculating program.

B. Aperture Efficiency

Based upon the projected area of the 6-rib hexagon, the hybrid-fed feed yielded an efficiency of 48.9%. The column supported circular cupped turnstile in the same reflector yielded an efficiency of 54.0%.

For the 8-rib octagon shaped aperture, the column supported circular cupped turnstile yielded an efficiency of 54.8%.

[3]In fact, there is no dc conductivity between gores due to the dielectric of the mylar and tape.

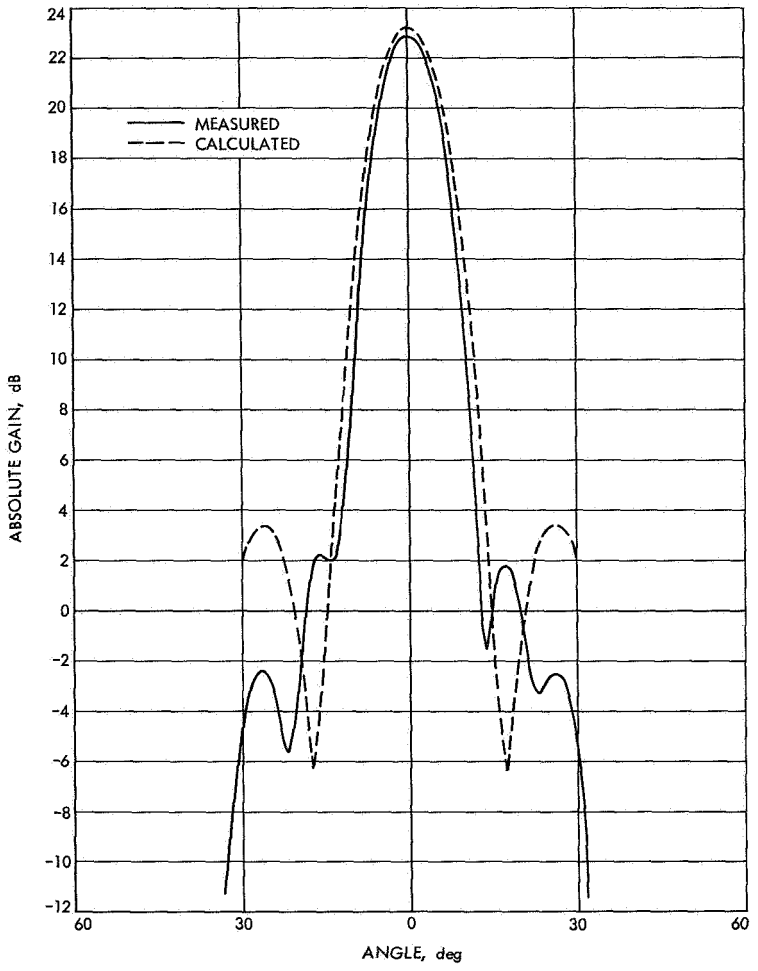

Fig. 7. Measured and calculated 6-rib dish patterns

The above measured overall efficiencies are the results of the product of the basic feed efficiency, feed blockage factor and the reflector surface efficiency. For the hybrid-fed feed for example, the physical blocked area is 4.4% of the total aperture area. Assuming that the measured gain (22.87 dB) and the calculated no blockage gain (23.21 dB) are correct, the blockage loss is 0.34 dB. This value is comparable with the minimum loss calculated value (0.39 dB) based upon Eq. (4) of Ref. 12. The actual blockage loss is expected to be slightly greater due to the tapered illumination.

C. Erectable Surface Loss

The ideal test to determine the loss of gain caused by the approximated parabolic surface would consist of comparing the peak gain of the erectable antenna and a true parabolic antenna using the same feed. Since a parabolic antenna was not available for measurement, a short computer program (shown in Appendix B) was written to calculate the on-axis gain of a perfect paraboloid using the surface current integration technique.

The program formulation is considerably simplified for a rotationally symmetric surface and the on-axis gain only. Figure 9 shows the illuminator aperture efficiency as a function of the paraboloid focal length to diameter ratio for both the circular cupped turnstile feed and the hybrid fed feed.

Based upon calculations using the hybrid-fed feed in the 6-rib dish the no blockage, peak gain of the erectable surface is 23.21 dB. The no-blockage gain of a perfect paraboloid of the same (10.36 in.) focal length using the same feed pattern and a diameter (32.7 in.) to yield an equal projected aperture area is 23.67 dB. The calculated surface loss is the difference of the two gains which is 0.46 dB. The calculated surface loss for the 8-rib reflector is 0.86 dB.

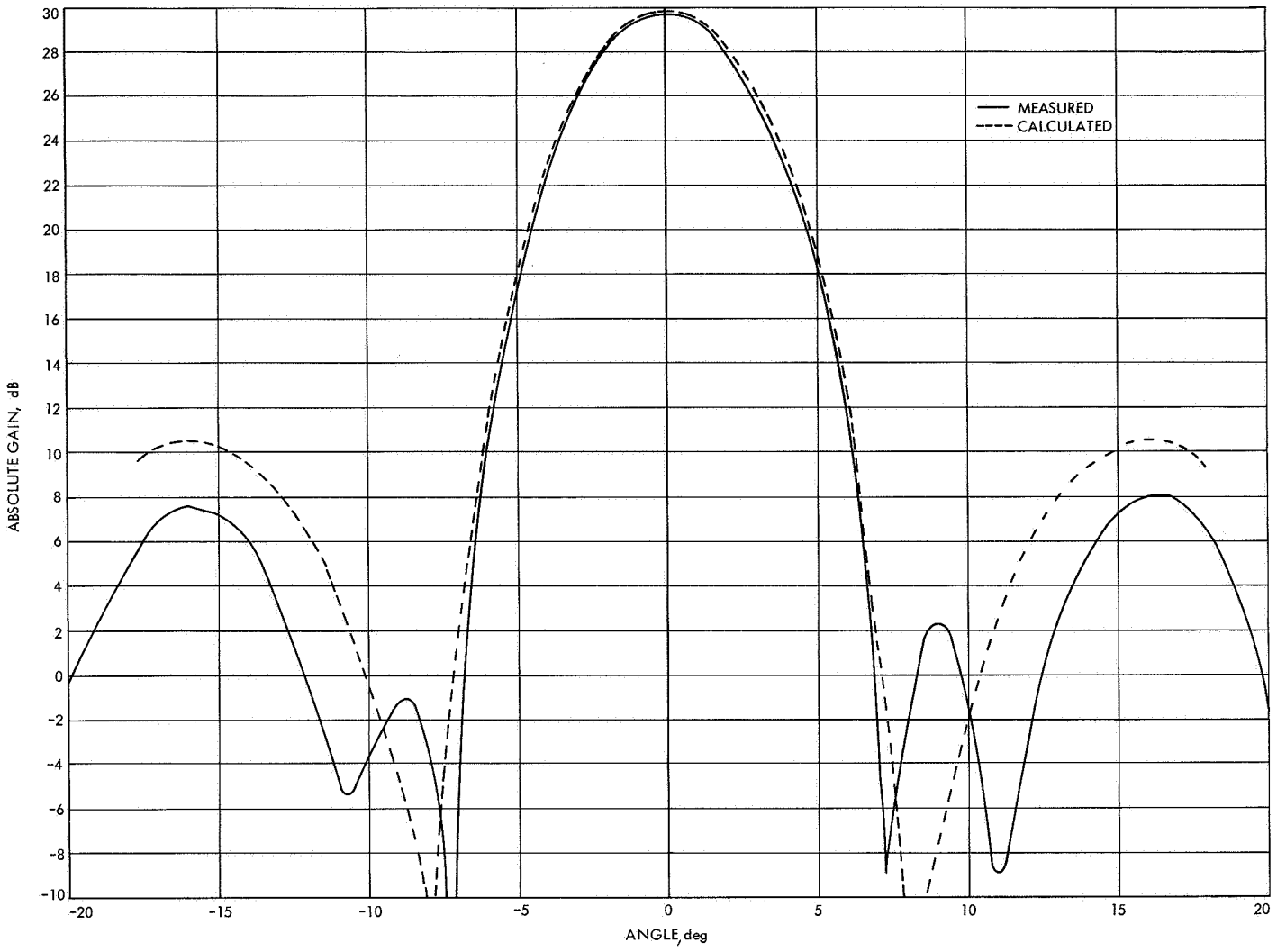

Fig. 8. Measured and calculated 8-rib dish patterns

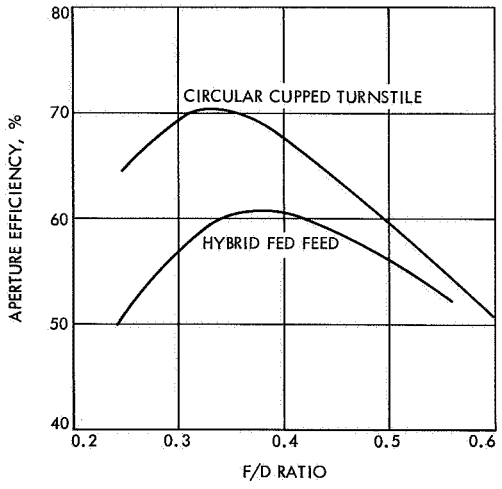

Fig. 9. Illuminator aperture efficiency in a perfect paraboloid

The surface loss is a function of the combination of both the primary illumination as well as the reflector configuration. Large deformations that are not strongly illuminated do not contribute greatly to gain loss.

From the best focus location program for the bybrid-fed feed in the 6-rib dish, the illumination weighted mean-square phase error is 0.325 rad^2 and the non-weighted peak error is 1.7 rad. The relation (Ref. 11) that the fractional loss of gain is equal to the weighted mean-square phase error evidently does not hold for the large deformations present in the 6-rib erectable model. The low surface loss value is surprising in view of the large phase errors.

For the cupped turnstile feed in the 8-rib model the weighted mean-square phase error is 0.314 rad^2 and the non-weighted peak phase error is 1.8 rad.

Based upon previous theoretical calculations (Ref. 13), which did not include provisions for relocating the focus for best gain, a more realistic expression for surface efficiency is given by

$$\eta_s = \exp -\left(K\frac{D_\lambda}{n^2}\right)^2 \tag{7}$$

where η_s is defined as the ratio of the peak gain of an equal aperture area radial ribbed reflector to a perfect paraboloid when both are illuminated by the same feed, D_λ is the diameter along a rib in wavelengths, and n is the number of ribs. K is a constant for a given type feed pattern as previously mentioned: for the hybrid fed feed, $K = 1.68$; for the cupped turnstile, $K = 2.0$.

The formula is not exact but should be satisfactory for initial design optimization studies wherein it is desired to optimize the spacecraft antenna gain to weight ratio.

V. Conclusions and Recommendations

The mathematical formulation required to calculate the circularly polarized secondary patterns of an erectable antenna surface have been developed. However, improvements in programming such as incorporating Ludwig's integration scheme and providing for generalized surface boundaries are needed. The existing program is structured to handle only one type erectable surface, the radial parabolic rib reflector with singly curved gores. Provisions are made, however, for varying the number of ribs, the focus position, the diameter, and the rib F/D ratio.

A method of determining the theoretical focus position for greatest gain with a given feed pattern and reflecting surface has been developed. In short (2λ) focal length reflectors, the method is limited in practice by reflector reaction on the feed. Additional study of reflector reaction on feeds is needed.

An improved expression (Eq. 7) for the surface loss due to approximating a parabolic reflector by the theoretical radial rib technique was obtained. In practice, fabric type reflective material will probably be used instead of the aluminized mylar. The resulting *upholstery effect* will produce a different surface. Surface equations need to be derived for this condition and other types of erectable antennas under free space conditions.

Appendix A
Equations

The following equations were derived in the course of the study. All equations are based upon the coordinate system of Fig. 1.

(1) Surface-position vector magnitude for radial ribbed reflector gore with displaced focus, F'.

$$\rho(\theta,\phi)=\frac{-2F'\sec\theta}{1+\left[1+\frac{F'}{F}\frac{\cos^2\left(\frac{\pi}{n}-\phi\right)}{\cos^2\left(\frac{\pi}{n}\right)}\tan^2\theta\right]^{1/2}} \tag{A-1}$$

n = number of ribs

F = parabolic rib focal length

F' = axially displaced focal length, $F' < F$

(2) Rib edge angle calculated from displaced focus.

$$\theta_E=\pi-\tan^{-1}\frac{0.5}{\left(\frac{F'}{D}\right)-\frac{1}{16(F/D)}} \tag{A-2}$$

(3) Gore center line edge angle.

$$\theta_{EM}=\pi-\tan^{-1}\frac{\cos\left(\frac{\pi}{n}\right)}{2\left[\left(\frac{F'}{D}\right)-\frac{1}{16(F/D)}\right]} \tag{A-3}$$

(4) Reflector edge boundary angle ϕ_B, measured from gore center line as a function of θ.

$$\phi_B(\theta)=\cos^{-1}\frac{\cos\left(\frac{\pi}{n}\right)}{2\left[\left(\frac{F'}{D}\right)-\frac{1}{16(F/D)}\right]\tan(\pi-\theta)} \tag{A-4}$$

(5) Reflector edge boundary angle θ_{EP} as a function of ϕ.

$$\theta_{EP}(\phi)=\tan^{-1}\frac{-\cos\left(\frac{\pi}{n}\right)}{2\left[\left(\frac{F'}{D}\right)-\frac{1}{16(F/D)}\right]\cos\left(\frac{\pi}{n}-\phi\right)} \tag{A-5}$$

(6) Parabolic rib arc length from vertex to $\theta = 3\pi/4$, and θ measured from displaced focus.

Let

$$x=2F\left[\left(1+\frac{F'}{F}\right)^{1/2}-1\right] \tag{A-6}$$

$$S_{135}=\frac{x}{2}\left(\frac{x^2}{4F^2}+1\right)^{1/2}+F\ln\left[\frac{x}{2F}+\left(\frac{x^2}{4F^2}+1\right)^{1/2}\right] \tag{A-7}$$

(7) Axial deviation of gore centerline from rib parabola at reflector edge.

$$\Delta=\frac{D\sin^2\left(\frac{\pi}{n}\right)}{16(F/D)} \tag{A-8}$$

(8) Focal length for equivalent cylindrical parabola of gore section.

$$F_c=F\cos^2\left(\frac{\pi}{n}\right) \tag{A-9}$$

(9) Gore panel layout pattern (see Fig. A-1).

Define

$$r=\alpha r_{max},\qquad 0\leq\alpha\leq 1,\qquad r_{max}=\frac{D}{2}\cos\left(\frac{\pi}{n}\right) \tag{A-10}$$

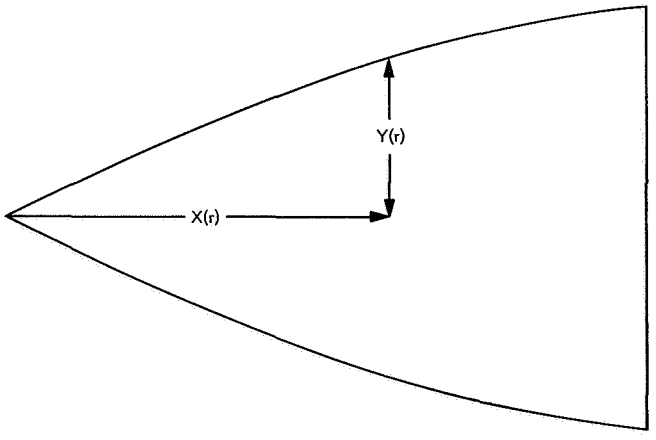

Fig. A-1. Gore panel layout pattern

$$X(r) = \frac{r}{2}\left\{\left[\frac{\sec^2\left(\frac{\pi}{n}\right)}{2F}\right]^2 r^2 + 1\right\}^{1/2}$$

$$+ \frac{F}{\sec^2\left(\frac{\pi}{n}\right)} \ln\left(\frac{r\sec^2\left(\frac{\pi}{n}\right)}{2F} + \left\{\left[\frac{\sec^2\left(\frac{\pi}{n}\right)}{2F}\right]^2 r^2 + 1\right\}^{1/2}\right) \tag{A-11}$$

$$Y(r) = r\tan\left(\frac{\pi}{n}\right) \tag{A-12}$$

To derive the equation of the gore surface refer to Fig. A-2. The same z-height or elevation of the surface with respect to the x-y plane may be obtained by either

$$z = \rho\cos\theta \tag{A-13}$$

or

$$z = r\cos\theta', \qquad r = |\mathbf{r}_1| = |\mathbf{r}_2| \tag{A-14}$$

Equating Eqs. (A-13) and (A-14) and solving for ρ yields

$$\rho = r\frac{\cos\theta'}{\cos\theta} \tag{A-15}$$

Thus, the magnitude of the surface position vector at angle θ is equal to the magnitude of the rib position vector at angle θ' times the ratio of the cosines of θ' and θ.

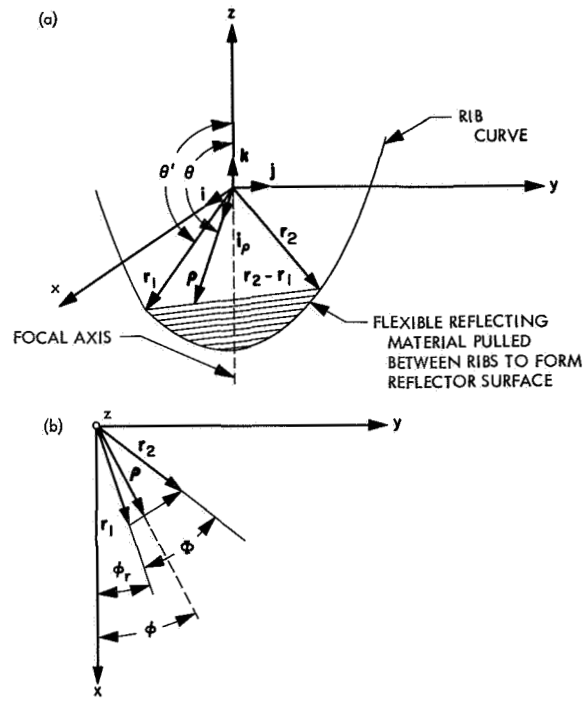

Fig. A-2. Gore geometry of a gored surface

A connective relation between θ and θ' is given by the triple scalar product

$$\boldsymbol{\rho}\cdot\mathbf{r}_1 \times \mathbf{r}_2 \tag{A-16}$$

wherein the cross product of $\mathbf{r}_1$ and $\mathbf{r}_2$ defines the normal vector to the plane containing $\mathbf{r}_1$ and $\mathbf{r}_2$. Since $\boldsymbol{\rho}$ also lies in this plane, by definition of the surface, then

$$\boldsymbol{\rho}\cdot\mathbf{r}_1 \times \mathbf{r}_2 \equiv 0 \tag{A-17}$$

With reference to Fig. A-2, substituting

$$\boldsymbol{\rho} = \rho(\sin\theta\cos\phi\mathbf{i} + \sin\theta\sin\phi\mathbf{j} + \cos\theta\mathbf{k}) \tag{A-18}$$

$$\mathbf{r}_1 = r(\sin\theta'\cos\phi_r\mathbf{i} + \sin\theta'\sin\phi_r\mathbf{j} + \cos\theta'\mathbf{k}) \tag{A-19}$$

and

$$\mathbf{r}_2 = r[\sin\theta'\cos(\phi_r + \Phi)\mathbf{i} + \sin\theta'\sin(\phi_r + \Phi)\mathbf{j} + \cos\theta'\mathbf{k}] \tag{A-20}$$

into Eq. (A-17) yields

$$\sin\theta\cos\theta'[\sin(\phi_r - \phi) + \sin(\phi - \phi_r - \Phi)] + \sin\theta'\cos\theta\sin\Phi = 0 \tag{A-21}$$

where Φ is the gore angular width and ϕ is the general azimuth angle between ϕ_r and $\phi_r + \Phi$. θ' and ϕ_r are, in general, functions of s, the arc length along the rib curve.

From Eq. (A-21)

$$\tan\theta' = \tan\theta \frac{\sin(\phi - \phi_r) + \sin(\Phi + \phi_r - \phi)}{\sin\Phi} \tag{A-22}$$

Using

$$\cos\theta' = \pm(1 + \tan^2\theta')^{-1/2} \tag{A-23}$$

or

$$\theta' = \cos^{-1} \pm \left\{1 + \tan^2\theta \left[\frac{\sin(\phi - \phi_r) + \sin(\Phi + \phi_r - \phi)}{\sin\Phi}\right]^2\right\}^{-1/2} \tag{A-24}$$

from which

$$\frac{\cos\theta'}{\cos\theta} = \left\{\cos^2\theta + \sin^2\theta \left[\frac{\sin(\phi - \phi_r) + \sin(\Phi + \phi_r - \phi)}{\sin\Phi}\right]^2\right\}^{-1/2} \tag{A-25}$$

or

$$\frac{\cos\theta'}{\cos\theta} = (\cos^2\theta + m^2\sin^2\theta)^{-1/2} \tag{A-26}$$

with

$$m = \frac{\sin(\phi - \phi_r) + \sin(\Phi + \phi_r - \phi)}{\sin\Phi} = \sec\Phi/2\cos(\phi_r + \Phi/2 - \phi) \tag{A-27}$$

Thus, Eq. (A-15) becomes in vector form

$$\boldsymbol{\rho} = \left[\frac{\mathbf{r}(s)\cdot\mathbf{r}(s)}{\cos^2\theta + m^2\sin^2\theta}\right]^{1/2}\mathbf{i}_\rho \tag{A-28}$$

For the radial ribbed reflectors considered at present, most of the rib curves are monotonic functions of θ'. That is, the rib curve position vector magnitude is a single valued function of θ'. With these restrictions, the magnitude of the rib curve position vector $|\mathbf{r}(s)|$ may be given as a function of θ', rather than as a function of arc length s, along the rib curve. Then, by use of Eq. (A-24), the rib curve position vector may be obtained in terms of θ.

Eq. (A-28), with the value of m substituted, becomes

$$\boldsymbol{\rho}(\theta, \phi) = r(\theta')\left[\cos^2\theta + \sin^2\theta\sec^2\Phi/2\cos^2(\phi_1 + \Phi/2 - \phi)\right]^{-1/2}\mathbf{i}_\rho \tag{A-29}$$

with $\phi_1 = \phi_r$, a constant for radial ribs.

For example, the polar equation of a parabolic rib is given by

$$r(\theta) = \frac{2F}{1 - \cos\theta} \tag{A-30}$$

where F is the focal length measured from the origin of coordinates of Fig. A-2 in the $-Z$ direction. θ is measured from the $+Z$ axis.

Using Eq. (A-24),

$$r(\theta') = \frac{2F}{1 \pm [1 + \sec^2 \Phi/2 \cos^2 (\phi_1 + \Phi/2 - \phi) \tan^2 \theta]^{-1/2}} \tag{A-31}$$

and substituting Eq. (A-31) in Eq. (A-29) yields

$$\boldsymbol{\rho}(\theta, \phi) = \frac{-2F \sec \theta}{[1 + \sec^2 \Phi/2 \cos^2 (\phi_1 + \Phi/2 - \phi) \tan^2 \theta]^{1/2} + 1} \mathbf{i}_\rho \tag{A-32}$$

as the surface position vector equation for the gore of a reflector whose ribs are purely radial and have a parabolic section.

Similarly, as further examples, for the straight rib shown in Fig. A-3

$$r(\theta) = \frac{F \tan \beta}{\sin \theta - \cos \theta \tan \beta} \tag{A-33}$$

and

$$\boldsymbol{\rho}(\theta, \phi) = \frac{-F \tan \beta}{\sec \Phi/2 \cos (\phi_1 + \Phi/2 - \phi) \sin \theta + \cos \theta \tan \beta} \mathbf{i}_\rho \tag{A-34}$$

For the circular rib of radius a, shown in Fig. A-4

$$r(\theta) = (a - F) \cos \theta + [a^2 - (a - F)^2 \sin^2 \theta]^{1/2} \tag{A-35}$$

and

$$\boldsymbol{\rho}(\theta, \phi) = \frac{-(a - F) + (\sec^2 \Phi/2 \cos^2 (\phi_1 + \Phi/2 - \phi) \tan^2 \theta [a^2 - (a - F)^2] + a^2)^{1/2}}{\cos \theta [1 + \sec^2 \Phi/2 \cos^2 (\phi_1 + \Phi/2 - \phi) \tan^2 \theta]} \mathbf{i}_\rho \tag{A-36}$$

The surface current vector (Eq. 74C of Ref. 1) is

$$\mathbf{I} = \int_S \frac{[G_L(\theta, \phi)]^{1/2}}{\rho} [\mathbf{n} \times (\boldsymbol{\rho}_1 \times \mathbf{e}_i)] \times \exp [-jk(\rho - \boldsymbol{\rho} \cdot \mathbf{R}_1)] \, dS \tag{A-37}$$

where

$G_L(\theta, \phi)$ = left-hand circularly polarized (LHCP) gain function of the illuminator

$\boldsymbol{\rho}_1 = \mathbf{i}_\rho$ = unit vector in the direction of increasing ρ

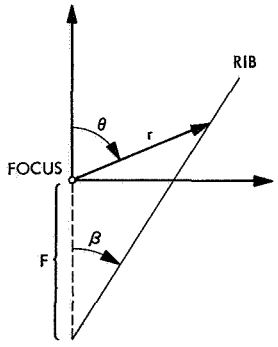

Fig. A-3. The straight-rib geometry

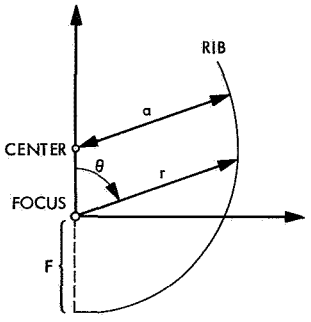

Fig. A-4. The circular-rib geometry

Similarly, for the θ, ϕ directions, the unit vectors are $\mathbf{i}_\theta$ and $\mathbf{i}_\phi$.

The magnitude of the surface position vector in terms of θ and ϕ is $\rho = \rho(\theta, \phi)$, and $k = 2\pi/\lambda$. The surface position vector is

$$\boldsymbol{\rho} = \rho(\theta, \phi)\, \mathbf{i}_\rho \tag{A-38}$$

The unit surface normal is

$$\mathbf{n} = \frac{\dfrac{\partial \boldsymbol{\rho}}{\partial \phi} \times \dfrac{\partial \boldsymbol{\rho}}{\partial \theta}}{(EG - F^2)^{1/2}} \tag{A-39}$$

The element of surface area is

$$dS = (EG - F^2)^{1/2}\, d\theta\, d\phi \tag{A-40}$$

where

$$E = \frac{\partial \boldsymbol{\rho}}{\partial \theta} \cdot \frac{\partial \boldsymbol{\rho}}{\partial \theta}, \qquad F = \frac{\partial \boldsymbol{\rho}}{\partial \theta} \cdot \frac{\partial \boldsymbol{\rho}}{\partial \phi}, \qquad G = \frac{\partial \boldsymbol{\rho}}{\partial \phi} \cdot \frac{\partial \boldsymbol{\rho}}{\partial \phi} \tag{A-41}$$

Equations (39–41) are obtained from differential geometry (Ref. 3), and the common radical term which will cancel out arises from the first fundamental form for a surface.

The unit vector defining the polarization of the illuminator electric field directed toward the reflector is given in terms of a unit LHCP vector (Ref. 5) as

$$\mathbf{e}_i = \boldsymbol{\mu}_L = 2^{-1/2}(\mathbf{i}_\theta + j\mathbf{i}_\phi) \exp -j\phi, \qquad \text{for } 0 < \theta \leqq \pi, \quad \text{any } \phi \tag{A-42}$$

The vector partial derivatives encountered in meeting requirement 2 are

$$\frac{\partial \boldsymbol{\rho}}{\partial \phi} = \rho \frac{\partial \mathbf{i}_\rho}{\partial \phi} + \frac{\partial \rho}{\partial \phi}\mathbf{i}_\rho = \rho \sin\theta\, \mathbf{i}_\phi + \frac{\partial \rho}{\partial \phi}\mathbf{i}_\rho \tag{A-43}$$

and

$$\frac{\partial \boldsymbol{\rho}}{\partial \theta} = \rho \frac{\partial \mathbf{i}_\rho}{\partial \theta} + \frac{\partial \rho}{\partial \theta}\mathbf{i}_\rho = \rho \mathbf{i}_\theta + \frac{\partial \rho}{\partial \theta}\mathbf{i}_\rho \tag{A-44}$$

The indicated vector operations of Eq. (A-37) may be expanded as

$$[\mathbf{n} \times (\mathbf{i}_\rho \times \boldsymbol{\mu}_L)] = (\mathbf{n} \cdot \boldsymbol{\mu}_L)\, \mathbf{i}_\rho - (\mathbf{n} \cdot \mathbf{i}_\rho)\, \boldsymbol{\mu}_L \tag{A-45}$$

The unit vector in the far field or **R** direction is given in terms of the unit cartesian coordinate vectors as

$$\mathbf{R}_1 = \sin\Theta\cos\Phi\, \mathbf{i}_x + \sin\Theta\sin\Phi\, \mathbf{i}_y + \cos\Theta\, \mathbf{i}_z \tag{A-46}$$

with

$$\mathbf{i}_\rho = \sin\theta\cos\phi\, \mathbf{i}_x + \sin\theta\sin\phi\, \mathbf{i}_y + \cos\theta\, \mathbf{i}_z \tag{A-47}$$

The phase term of Eq. (A-37) becomes

$$\begin{aligned}(\rho - \boldsymbol{\rho} \cdot \mathbf{R}_1) &= \rho(1 - \mathbf{i}_\rho \cdot \mathbf{R}_1) \\ &= \rho[1 - \sin\theta\sin\Theta\cos(\Phi - \phi) - \cos\theta\cos\Theta]\end{aligned} \tag{A-48}$$

Thus, for LHCP illumination incident upon the reflector, the surface current vector (Eq. A-37) becomes

$$\begin{aligned}\mathbf{I} = \int_S \left[\frac{G_L(\theta, \phi)}{2}\right]^{1/2} &\left[\left(\frac{\partial \rho}{\partial \theta}\sin\theta + j\frac{\partial \rho}{\partial \phi}\right)\mathbf{i}_\rho + \rho\sin\theta\,(\mathbf{i}_\theta + j\mathbf{i}_\phi)\right] \exp -j\phi \\ &\times \exp\left\{-j\frac{2\pi}{\lambda}\rho[1 - \sin\theta\sin\Theta\cos(\Phi - \phi) - \cos\theta\cos\Theta]\right\} d\theta\, d\phi\end{aligned} \tag{A-49}$$

To obtain an integral of only the portion of the surface current that contributes to the RHCP far field in the (Θ, Φ) direction, dot Eq. (A-49) above with the complex conjugate of the RHCP far field polarization vector; namely,

$$\boldsymbol{\mu}_R'^{*} = 2^{-1/2} \exp -j\Phi \begin{Bmatrix} [\sin\theta\cos\Theta\cos(\Phi - \phi) - \cos\theta\sin\Theta]\, \mathbf{i}_\rho & [-\sin\theta\sin(\Phi - \phi)]\, \mathbf{i}_\rho \\ [\cos\theta\cos\Theta\cos(\Phi - \phi) + \sin\theta\sin\Theta]\, \mathbf{i}_\theta + j & [-\cos\theta\sin(\Phi - \phi)]\, \mathbf{i}_\theta \\ [\cos\Theta\sin(\Phi - \phi)]\, \mathbf{i}_\phi & [\cos(\Phi - \phi)]\, \mathbf{i}_\phi \end{Bmatrix},$$

$$\text{for } 0 \leqq \Theta < \pi, \qquad \text{any } \Phi \tag{A-50}$$

which yields

$$I = \int_s \frac{[G_L(\theta,\phi)]^{1/2}}{2} \Bigg[\sin\theta \left\{ \frac{\partial\rho}{\partial\phi} \sin(\Phi-\phi) + \rho\cos(\Phi-\phi)(\cos\theta\cos\Theta - 1) + \sin\Theta\left(\rho\sin\theta - \frac{\partial\rho}{\partial\theta}\cos\theta\right) \right.$$

$$\left. + \frac{\partial\rho}{\partial\theta}\sin\theta\cos\Theta\cos(\Phi-\phi) \right\} + j\left\{ \frac{\partial\rho}{\partial\phi}[\sin\theta\cos\Theta\cos(\Phi-\phi) - \cos\theta\sin\Theta] - \sin\theta\sin(\Phi-\phi) \right.$$

$$\left. \times \left[\frac{\partial\rho}{\partial\theta}\sin\theta + \rho(\cos\theta - \cos\Theta) \right] \right\} \Bigg] \exp -j(\phi+\Phi) \exp\left\{ -j\frac{2\pi}{\lambda}\rho[1 - \sin\theta\sin\Theta\cos(\Phi-\phi) - \cos\theta\cos\Theta] \right\} d\theta\, d\phi \tag{A-51}$$

The total RHCP gain in the (Θ, Φ) direction is obtained by adding the surface current scattered radiation to the direct feed RHCP radiation in the desired direction:

$$G_R = \left| [G_R(\Theta,\Phi)]^{1/2} - \frac{jI}{\lambda} \right|^2 \qquad \text{Q.E.D.} \tag{A-52}$$

Appendix B

Computer Programs

I. Pattern Calculating Program

The program comment cards generally make the programs self explanatory. However, in Program I, the mathematical development for the surface current integrand expression [FTP (N) = Amplitude, PTP (N) = Phase, in the program] is given in the appendix extracted from JPL Space Programs Summary (SPS) 37-47, Vol. III. The surface equation [R (I, J) in the program] developed for a displaced focus (Equation 1, Appendix A of this report) follows the derivation given in Appendix A which was extracted from SPS 37-35, Vol. IV.

The printing of SS1 and SS2 in statement number 89 represents the cumulative sum of the real and imaginary part of the surface current contribution of the reflector gores to the total pattern. This printing can be omitted to save time if desired by removing the write and format cards.

```
                                JPL,J358000,33916-0,18416,A  IC      IBJOB L10MKC  7094 A
          HARDY      -  EFN   SOURCE STATEMENT  -  IFN(S)  -

C              IGAIN RADIAL RIBBED, AXIAL FOCUS DISPLACEMENT   RMD 014
C              USING APPROXIMATE EQUAL AREA POINTS ON SURFACE
C                    DIA=RIB DIAMETER IN WAVELENGTHS
C                  SHAPE=RIB F/D RATIO
C                   RIBS=NUMBER OF RIBS OR GORES
C                     ZA=FOCUS DISPLACEMENT TOWARD VERTEX IN WAVELENGTHS
C                    TCI=OUTPUT ANGULAR INCREMENT-THETA
C                    PCI=OUTPUT ANGULAR INCREMENT-PHI
C                    NTC=NUMBER OF THETA OUTPUTS
C                    NPC=NUMBER OF PHI OUTPUTS
C                     NT=NUMBER OF RADIAL SURFACE DIVISIONS
C                     PK=RATIO OF THETA TO PHI ARC LENGTH INCREMENTS
C                     FR=FEED PATTERN GAIN IN DB
   99 READ(5,1)DIA,SHAPE,RIBS,ZA                                          1
    1 FORMAT(4F10.2)
      READ(5,2)TCI,PCI,NTC,NPC                                             2
    2 FORMAT(2F10.2,2I2)
      READ(5,3)PK,NT                                                       5
    3 FORMAT(1F10.2,1I2)
      WRITE(6,98)DIA,SHAPE,RIBS,ZA                                         7
  980FORMAT(6H DIA =,F10.3,2X,6H F/D =,F10.3,2X,7H RIBS =,F10.3,2X,20H
     1AXIAL FEED OFFSET =,F10.3)
      WRITE(6,97)NT,PK                                                     8
  970FORMAT(21H NO. OF RADIAL DIV. =,I4,2X,29H THETA/PHI ARC LENGTH RAT
     1IO =,F10.2)
      ODIMENSION SX(2),SA(2),T(61),R(61,31),MP(31),P(61,31),DRT(61,31),
     1DRP(61,31),S(3,2),FTP(3),PTP(3),FR(61)
      IRIBS=RIBS
      E=3.14159/180.
C               RIB EDGE ANGLE CALCULATED FROM DISPLACED FOCUS, FP
      FP=(DIA*SHAPE)-ZA
      FZ=(FP/DIA)-(1./(16.*SHAPE))
      TE=3.14159-ATAN2(.5,FZ)                                              10
      T(1)=TE
C               APPROXIMATE EQUIAREA THETA GENERATOR ROUTINE
      FOC=DIA*SHAPE
C               SX(1)FOR MAXIMUM RIB ARC LENGTH
C               SX(2) FOR VERTEX TO 135 DEGREES
      SX(1)=0.5*DIA
      SX(2)=2.*FOC*(-1.+SQRT(1.+(FP/FOC)))                                 11
      DO 4 I=1,2
   40SA(I)=0.5*SX(I)*SQRT(1.+(SX(I)*SX(I)/(4.*FOC*FOC)))+FOC
     1*ALOG((.5*SX(I)/FOC)+SQRT(1.+(SX(I)*SX(I)/(4.*FOC*FOC))))
C               QUADRATIC COEFFICIENTS FOR THETA
C               IN TERMS OF NORMALIZED ARC LENGTH                       18
      AS=((3.*3.14159/4.)*SA(1)-TE*SA(2)-3.14159*(SA(1)-SA(2)))/(SA(1)*
     1SA(2)*(SA(2)-SA(1)))
      BS=(TE-3.14159-AS*SA(1)*SA(1))/SA(1)
C               GENERATE MAJOR RADIAL INCREMENTS
      NT2=2*NT
      AT2=NT2
      DO 5 I=1,NT2,2
      L=I+2
      BI=I+1
   50T(L)=(AS*SA(1)*SA(1)*(AT2-BI)*(AT2-BI)/(AT2*AT2))+(BS*SA(1)*(AT2-
```

```
                                JPL,J358000,33916-0,18416,A  IC      IBJOB L10MKC  7094 A
          HARDY      -  EFN   SOURCE STATEMENT  -  IFN(S)  -

     1BI)/(AT2))+3.14159
C                GENERATE EQUAL SPACED SUB RADIAL INCREMENTS
      DO 6 I=2,NT2,2
    6 T(I)=T(I-1)+0.5*(T(I+1)-T(I-1))
C                APPROXIMATE EQUIAREA PHI GENERATOR ROUTINE
C                SURFACE POSITION VECTOR MAGNITUDES ALONG A RIB
C                FOR PHI ARC LENGTH
      NT3=NT2+1
      DO 7 I=1,NT3
CIRCUPTNX W/COLUMN FEED PATTERN IN DB VS) RADIANS CONE ANGLE
      FR(I)=-3.418*T(I)*T(I)+23.98*T(I)-33.88
    7OR(I,1)=(-2.*FP/COS(T(I)))/(1.+SQRT(1.+(FP/FOC)*TAN(T(I))*TAN(T(I
     1))))
C                NUMBER OF PHI INCREMENTS IN GORE WIDTH
C                AS A FUNCTION OF THETA = MP(I)                          54
      PH=3.14159/RIBS
      ANT=NT
      TEM=3.14159-ATAN2(COS(PH),2.*FZ)
C.               EXCLUDING PHI GAPS AT REFLECTOR EDGE                    63
      DO 8 I=1,NT2
      IF(T(I)-TEM)9,10,10
    9 PB=ARCOS(COS(PH)/(2.*FZ*TAN(3.14159-T(I))))                         71
   12 AP=((PH)-PB)*R(I,1)*SIN(T(I))*ANT*PK/SA(1)                          77
      IP=AP+1.
      MK=(2*IP)+1
      MP(I)=2*MK
      DO 14 J=1,MK
      AJ=J
      AMK=MK
      P(I,J)=(AJ-1.)*((PH)-PB)/(AMK-1.)
      JK=J+MK
   14 P(I,JK)=(PH)+PB+P(I,J)
      GO TO 8
   10 AP=R(I,1)*SIN(T(I))*(2.*PH)*ANT*PK/SA(1)                            92
      IP=AP+1.
      MP(I)=(2*IP)+1
      MK=MP(I)
      DO 15 J=1,MK
      AMK=MK
      AJ=J
   15 P(I,J)=(AJ-1.)*(2.*PH)/(AMK-1.)
    8 CONTINUE
      WRITE(6,85)TE,SA(1),T(2),P(2,2)                                     105
   85OFORMAT(5H TE =,F10.3,2X,8H SA(1) =,F10.3,2X,7H T(2) =,F10.3,2X,9H
     1P(2,2) =,F10.3)
C                CALCULATE SURFACE POSITION VECTOR MAGNITUDES
C                AND SURFACE DERIVATIVES ANALYTICALLY
      DO 16 I=2,NT2
      MK=MP(I)
      CT=1./COS(T(I))                                                     112
      TT=TAN(T(I))                                                        114
      DO 16 J=1,MK
      CP=COS((PH)-P(I,J))                                                 118
      SP=SIN((PH)-P(I,J))                                                 120
      CD=COS(PH)                                                          121
      RDR=SQRT(1.+(FP/FOC)*(CP*CP/(CD*CD))*TT*TT)                         122
```

```
      RD=1.+RDR
      R(I,J)=-2.*FP*CT/RD
     ODRT(I,J)=((-2.*FP*CT*TT*RD)+(2.*FP*FP*CT*TT*CT*CT*CP*(CP/(RDR*CD*
     1CD*FOC))))/(RD*RD)
      DRP(I,J)=(2.*FP*CT*TT*TT*CP*SP*FP)/(FOC*RDR*RD*RD*CD*CD)
   16 CONTINUE
      MP(NT3)=3
      DO 165 J=1,3
      R(NT3,J)=FP
      DRT(NT3,J)=0.
  165 DRP(NT3,J)=0.
C               SURFACE CURRENT INTEGRAND CALCULATING ROUTINE
C               INITIALIZE OUTPUT ANGLE CALCULATION LOOPS
      II=1
   24 LL=1
C               CALCULATE INTEGRAND
      AI=II
      PC=(AI*PCI-PCI)*E
   25 AL=LL
      TC=(AL*TCI-TCI)*E
      C=COS(TC)                                                        143
      D=SIN(TC)                                                        144
      SS1=0.
      SS2=0.
C               INTEGRATE SURFACE CURRENT OVER ALL GORES
      DO 17 KK=1,IRIBS
      AKK=KK
      PG=2.*PH*(AKK-1.)
      WRITE(6,89)SS1,SS2                                               148
   89 FORMAT(6H SS1 =,F10.3,2X,6H SS2 =,F10.3)
      DO 18 L=1,3
      S(L,1)=0.
   18 S(L,2)=0.
C               INTEGRATE ALL THETA RADII
      DO 17 K=1,NT2,2
      DO 60 L=2,3
      I=L+K-1
      A=COS(T(I))                                                      160
      B=SIN(T(I))
C               INTEGRATE OVER PHI FOR EACH THETA                      162
   29 MK=MP(I)
      AMK=MK
      IF(TEM-T(I))33,33,56
   56 MK=MP(I)-3
   33 DO 60 M=1,MK,2
      AM=M
      DO 50 N=1,3
      IF(TEM-T(I))40,40,41
   41 IF(AM-(AMK/2.))40,42,42
   42 J=M+N
      GO TO 45
   40 J=M+N-1
   45 G=COS(PC-(PG+P(I,J)))                                            185
      H=SIN(PC-(PG+P(I,J)))                                            187
     OX= ((DRP(I,J)*H)+(R(I,J)*G*(A*C-1.))+((R(I,J)*B-DRT(I,J)*A))+(
     1DRT(I,J)*C*C*G))*B
```

```
                                JPL,J358000,33916-0,18416,A  IC      IBJOB L10MKC  7094 A
         HARDY      - EFN   SOURCE STATEMENT  -  IFN(S)  -

      IF(X)176,175,176
  175 X=.000001
  176 Y=(DRP(I,J)*(B*C*C-A*D))-((B*H)*(B*DRT(I,J)+(A-C)*R(I,J)))
      FTP(N)=SQRT(X*X+Y*Y)*0.5*EXP(0.115*FR(I))                              199
   500PTP(N)=ATAN2(Y,X)-(6.28318*R(I,J)*(1.-(B*D*G)-(A*C)))-(PG+P(I,J))
     1-PC
CSIMPSONS 1/3 INTEGRATION IN PHI                                             204
      FAC=FTP(1)*COS(PTP(1))                                                 209
      FAS=FTP(1)*SIN(PTP(1))                                                 210
      FBC=FTP(2)*COS(PTP(2))                                                 211
      FBS=FTP(2)*SIN(PTP(2))                                                 212
      FCC=FTP(3)*COS(PTP(3))                                                 213
      FCS=FTP(3)*SIN(PTP(3))                                                 214
      S(L,1)=S(L,1)+((P(I,2)/3.)*(FAC+4.*FBC+FCC))
   60 S(L,2)=S(L,2)+((P(I,2)/3.)*(FAS+4.*FBS+FCS))
C               SIMPSONS 1/3 INTEGRATION IN THETA
   61 SS1=SS1+(((T(I)-T(I-1))/3.)*(S(1,1)+4.*S(2,1)+S(3,1)))
      SS2=SS2+(((T(I)-T(I-1))/3.)*(S(1,2)+4.*S(2,2)+S(3,2)))
      S(1,1)=S(3,1)
      S(1,2)=S(3,2)
      S(2,1)=0.
      S(2,2)=0.
      S(3,1)=0.
   17 S(3,2)=0.
C               RELATIVE PHASE OF PATTERN WITH RESPECT TO FEED POINT
      PHASE=ATAN2(SS2/SS1)/E
C               GAIN WITH NO BLOCKAGE OR BACKLOBE CONTRIBUTION                 233
      DBGAIN=10.*ALOG10(SS1*SS1+SS2*SS2)                                     234
      PHI=PC/E
      THETA=TC/E
      WRITE(6,87)THETA,PHI,DBGAIN,PHASE                                      235
   870FORMAT(8H THETA =,F10.3,2X,6H PHI =,F10.3,2X,9H DBGAIN =,F10.3,
     18H PHASE =,F10.3)
      LL=LL+1
      IF(NTC-LL)26,25,25
   26 II=II+1
      IF(NPC-II)27,24,24
   27 GO TO 99
      END
```

II. Illumination Weighted Average Phase Deviation and rms, Phase Error vs Focus Displacement

In Program II, the third from last statement causes the program to increment the focus displacement axially toward the vertex from the original displacement ZA in ⅛-wavelength increments. The program gives as output not only the illumination weighted (WTDELA, WTSMSQ) average and rms phase deviations, but also their unweighted (DELAVE, RMSDEL) values. The maximum phase deviation (DELMAX) is also calculated for the particular focus displacement, ZA.

```
CALCULATED FOCAL POSITION FOR ZERO AVERAGE PHASE DEVIATION OVER APERTURE
CSING RANDOM SAMPLING OF SURFACE                                    RMD 016
C1620 PROGRAM
C  RIBS  = NUMBER OF RIBS
C  DIA   = RIB DIAMETER IN WAVELENGTHS
C  SHAPE = RIB FOCAL LENGTH TO DIAMETER RATIO, F/D
C  ZA    = FOCUS DISPLACEMENT TOWARD VERTEX IN WAVELENGTHS
C  NP    = NUMBER OF RANDOM SAMPLE POINTS
      READ 1,RIBS,DIA,SHAPE
    1 FORMAT(3F10.3)
   11 READ 2,ZA,NP
    2 FORMAT(1F10.3,1I3)
CRIB EDGE ANGLE CALCULATED FROM DISPLACED FOCUS, FP
      PI=3.14159
    4 FP=(DIA*SHAPE)-ZA
      FZ=(FP/DIA)-(1./(16.*SHAPE))
      TE=PI-ATANF(.5/FZ)
      FOC=DIA*SHAPE
      SUMDEL=0.0
      DELMOS=0.0
      DELA=0.0
      WTDEL=0.0
      WTSSM=0.0
    5 K=1
      X=58.3902
      COMMON X
CENERATE RANDOM THETA VALUE AND SCALE TO FIT REFLECTOR
    6 CALL RANDOM(I)
      QNR=I
      T=TE+((QNR/9999.)*(PI-TE))
CENERATE RANDOM PHI VALUE
      CALL RANDOM(I)
      QNL=I
      P=(QNL/9999.)*2.*PI
      L=P*RIBS/(2.*PI)
      AL=L
      PL=(2.*PI)*AL/RIBS
      PAL=PL-P+(PI/RIBS)
CEDGE TRIM CHECK
      TB=PI-ATANF((COSF(PI/RIBS))/(2.*FZ*COSF(PAL)))
      IF(T-TB)6,66,66
   66 R=(-2.*FP/COSF(T)) /(1.+SQRTF(1.+(FP/FOC)*SINF(T)*SINF(T)
     1*COSF(PAL)*COSF(PAL)/(COSF(T)*COSF(T)*COSF(PI/RIBS)*COSF(PI/
     2RIBS))))
      DEL=(2.*PI)*((2.*FP)-(R*(1.-COSF(T))))
CFEED ILLUMINATION WEIGHTING FACTOR, FT
CIRCUPTNX W/ COLUMN FEED
      FT=(FP/R)*EXPF(.115*(7.6-(-3.418*T*T+23.98*T-33.88)))
      ABDEL=ABSF(DEL)
      IF(DELMOS-ABDEL)88,89,89
   88 DELMOS=ABDEL
      DELMAX=DEL
   89 SQDEL=DEL*DEL
      DELA=DELA+DEL
      SUMDEL=SUMDEL+SQDEL
      WTDEL=WTDEL+(FT*DEL)
      WTSSM=WTSSM+(FT*SQDEL)
      K=K+1
      Q=NP-K
```

```
   IF(Q)7,6,6
 7 AUT=NP
   WTSMSQ=SQRTF(WTSSM/AUT)
   WTDELA=WTDEL/AUT
   RMSDEL=SQRTF(SUMDEL/AUT)
   DELAVE=DELA/AUT
   PRINT 3,RIBS,DIA,SHAPE,ZA,NP
 3 FORMAT(7H RIBS =,F10.3,2X,6H DIA =,F10.3,2X,6H F/D =,F10.3,2X,5H Z
  1A =,F10.3,2X,5H NP =,I4)
   PRINT 8,RMSDEL,DELAVE
 8 FORMAT(9H RMSDEL =,F6.4,2X,9H DELAVE =,F6.4)
   PRINT 45,DELMAX
45 FORMAT(9H DELMAX=,F10.3)
   PRINT 21,FP,WTDELA,WTSMSQ
21 FORMAT(5H FP =,F10.3,2X,28H WEIGHTED MEAN PHASE ERROR =,F10.3,2X,2
  19H WEIGHTED MEAN-SQUARE ERROR =,F10.3)
   ZA=ZA+0.125
   GO TO 4
   END
```

III. Feed Illumination Efficiency in Perfect Paraboloid

In Program III, the reflector diameter should be the diameter of a circular outline reflector that has the same aperture area as the erectable reflector when it is desired to use the program in the process of determining surface loss of an erectable reflector. The corresponding focal length to be used in inputting the shape or F/D ratio should be the best focal length determined from Program II. The third from last statement increments the F/D ratio in steps of 0.05.

```
CFEED EFFICIENCY IN PERFECT PARABOLOID BY SURFACE CURRENT INTEGRATION
C1620 PROGRAM                                                    RMD 017
C  DIA    = REFLECTOR DIAMETER IN WAVELENGTHS
C  SHAPE  = FOCAL LENGTH TO DIAMETER RATIO; F/D
C  AI     = FEED CUBIC COEFFICIENT (FOR FEED PATTERN IN DB AS A FUNCTION
C                                   (OF CONE ANGLE IN RADIANS)
C  BI     = FEED QUADRATIC COEFFICIENT
C  CI     = FEED LINEAR COEFFICIENT
C  DI     = FEED CONSTANT TERM
C  NT     = NUMBER OF ANGULAR INCREMENTS (ODD NUMBER REQUIRED)
      DIMENSION X(3)
      READ 1,DIA,SHAPE,NT
    1 FORMAT(2F10.3,I13)
      READ 2,AI,BI,CI,DI
    2 FORMAT(4F10.3)
   86 S=0.
      DO 4 I=1,3
    4 X(I)=0.
      PI=3.14159
      E=PI/180.
      ANT=NT-1
CEDGE ANGLE OF REFLECTOR
      TE=ATANF(.5/(SHAPE-(1./(16.*SHAPE))))
      NET=NT-2
CALCULATE INTEGRAND VALUES
      DO 8 L=1,NET,2
      DO 7 M=2,3
      I=L+M-1
      AB=I
      T=PI-((TE/ANT)*(AB-1.))
      Y=AI*T*T*T+(BI*T*T)+(CI*T)+DI
      YY=EXPF(0.115*Y)
    7 X(M)=YY*(SINF(T)/(1.-COSF(T)))
CPERFORM SIMPSONS 1/3 INTEGRATION
      S=S+((TE/(3.*ANT))*(X(1)+4.*X(2)+X(3)))
      X(1)=X(3)
      X(2)=0.
    8 X(3)=0.
CALCULATED GAIN = GAIN
      GAIN=(4.*PI*DIA*SHAPE*S)**2
CGAIN WITH UNIFORM ILLUMINATION
      GUNI =(PI*DIA)**2
CFEED ILLUMINATION EFFICIENCY = ETAFD
      ETAFD=GAIN/GUNI
      GFDB=4.34*LOGF(GAIN)
      GUDB=4.34*LOGF(GUNI)
      TEP=TE/E
      PRINT 3,DIA,SHAPE,NT
    3 FORMAT(6H DIA =,F10.3,2X,6H F/D =,F10.3,2X,5H NT =,I4)
      PRINT 11,TEP
   11 FORMAT (23H REFLECTOR EDGE ANGLE =,F10.3)
      PRINT 9,ETAFD,GFDB,GUDB
    9 FORMAT(8H ETAFD =,F10.3,2X,7H GFDB =,F10.3,2X,7H GUDB =,F10.3)
      SHAPE=SHAPE+.05
      GO TO 86
      END
```

References

1. Silver, S., *Microwave Antenna Theory and Design*, pp. 149–151. McGraw-Hill Book Co., Inc., New York, 1949.
2. Dickinson, R., "Large Aperture Antenna Study," in *Supporting Research and Advanced Development*, Space Programs Summary 37-35, Vol. IV, pp. 273–278. Jet Propulsion Laboratory, Pasadena, Calif., Oct. 31, 1965.
3. Lass, H., *Vector and Tensor Analysis*, pp. 70–88. McGraw-Hill Book Co., Inc., New York, 1950.
4. Eisenhart, L., *A Treatise on the Differential Geometry of Curves and Surfaces.* Ginn and Co., Boston, Mass., 1909.
5. Kales, M., "Part III, Elliptically Polarized Waves and Antennas—Complex Vector Representations of Elliptically Polarized Fields," *Proc. IRE*, pp. 544–549. May 1951.
6. Mathis, H., "A Short Proof that an Isotropic Antenna is Impossible," *Proc. IRE*, Vol. 39, p. 970, Aug. 1951.
7. Mathis, H., "On Isotropic Antennas," *Proc. IRE*, p. 1810, Dec. 1954.
8. Dickinson, R., "Spacecraft Antenna Research: Large Aperture Antennas," in *Supporting Research and Advanced Development*, Space Programs Summary 37-47, Vol. III, pp. 242–247. Jet Propulsion Laboratory, Pasadena, Calif., Oct. 31, 1967.
9. Allen, C., "Numerical Integration Methods for Antenna Pattern Calculations," *IRE Trans. Antennas Propagation* (special supplement), pp. 5387–5401, Dec. 1959.
10. Salvadori, M., and Baron, M., *Numerical Methods in Engineering*, pp. 176–178. Prentice Hall, Inc., 1952.
11. Ruze, J., "Antenna Tolerance Theory—A Review," *Proc. IEEE*, Vol. 54, No. 4, pp. 633–640, Apr. 1966.
12. Ludwig, A., "Efficient Antenna Systems: Aperture Blockage and Surface Tolerance Loss Calculations for Non-Uniform Illumination and Error Distribution," in *The Deep Space Network*, Space Programs Summary 37-41, Vol. III, pp. 89–90. Jet Propulsion Laboratory, Pasadena, Calif., Sept. 30, 1966.
13. Dickinson, R., "Large Aperture Antenna Study," in *Supporting Research and Advanced Development*, Space Programs Summary 37-45, Vol. IV, pp. 333–335. Jet Propulsion Laboratory, Pasadena, Calif., June 30, 1967.